

Determination of specific surface area of irregular aggregate by random sectioning and its comparison with conventional methods

Ren, Qiang; Ding, Luchuan; Dai, Xiaodi; Jiang, Zhengwu; Ye, Guang; De Schutter, Geert

DOI

[10.1016/j.conbuildmat.2020.122019](https://doi.org/10.1016/j.conbuildmat.2020.122019)

Publication date

2021

Document Version

Final published version

Published in

Construction and Building Materials

Citation (APA)

Ren, Q., Ding, L., Dai, X., Jiang, Z., Ye, G., & De Schutter, G. (2021). Determination of specific surface area of irregular aggregate by random sectioning and its comparison with conventional methods. *Construction and Building Materials*, 273, 1-9. Article 122019. <https://doi.org/10.1016/j.conbuildmat.2020.122019>

Important note

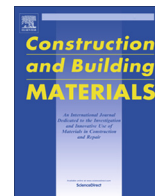
To cite this publication, please use the final published version (if applicable).
Please check the document version above.

Copyright

Other than for strictly personal use, it is not permitted to download, forward or distribute the text or part of it, without the consent of the author(s) and/or copyright holder(s), unless the work is under an open content license such as Creative Commons.

Takedown policy

Please contact us and provide details if you believe this document breaches copyrights.
We will remove access to the work immediately and investigate your claim.



Determination of specific surface area of irregular aggregate by random sectioning and its comparison with conventional methods

Qiang Ren^{a,b}, Luchuan Ding^b, Xiaodi Dai^b, Zhengwu Jiang^{a,*}, Guang Ye^{b,c}, Geert De Schutter^{b,*}

^a Key Laboratory of Advanced Civil Engineering Materials of Ministry of Education, School of Materials Science and Engineering, Tongji University, 4800 Cao'an Road, Shanghai 201804, China

^b Magnel-Vandepitte Laboratory, Department of Structural Engineering and Building Materials, Ghent University, Technologiepark-Zwijnaarde 60, Ghent 9052, Belgium

^c Microlab, Faculty of Civil Engineering and Geosciences, Delft University of Technology, Stevinweg 1, 2628 CN Delft, The Netherlands

HIGHLIGHTS

- An easy-to-perform method is proposed to determine SSA of irregular aggregate.
- The proposed method is reliable compared to CT.
- Difference among various methods is analyzed.
- Suggestions are provided for selecting proper testing method of SSA.

ARTICLE INFO

Article history:

Received 24 March 2020

Received in revised form 12 November 2020

Accepted 12 December 2020

Keywords:

Aggregates
Specific surface area
Random sectioning
Spherical assumption
BET
Computed tomography

ABSTRACT

A two-dimensional (2D) image-based methodology was proposed to measure the specific surface area (SSA, specified as the surface area per unit volume) of irregular aggregate by random sectioning. Conventional methods including spherical assumption, Brunauer-Emmett-Teller (BET) and computed tomography (CT) tests were used and compared in this study. Results show that spherical assumption provides the lowest SSA among these methods since the feature of anisotropy in dimension is not considered. SSA by BET test has one order of magnitude higher value than others, which is attributed to the fact that BET method measures each position of particles that nitrogen molecule can be adsorbed on during the applied relative pressure, based on the 'pixel' of nitrogen molecule. The proposed random sectioning method presents very similar SSA result compared to CT method, indicating that it can be considered as a reliable method. To improve the estimation of SSA by random sectioning method, factors that may influence SSA result were analyzed. Results indicate that the number of samples should be high enough to reach a constant result and the thresholding algorithm should be adequate. Besides, a higher resolution of pixel provides a higher SSA value. The comparison among these methods demonstrate that it is necessary to determine the scale at which the features of the surface are supposed to be captured before selecting the optimal testing method.

© 2020 Elsevier Ltd. All rights reserved.

1. Introduction

Among the various properties of aggregate, specific surface area (SSA) is a comprehensive evaluation of dimension, shape, angularity and surface roughness of aggregate [1,2]. From the viewpoint of mix design, SSA of aggregates influences the amount of surface to be wetted, hence the requirement of paste in concrete mixture, which influences the workability [3–5], mechanical properties

[6,7] and durability [8,9] of concrete. SSA determination of aggregates is thus a topic of great interest for concrete research.

The original estimation of SSA was based on empirical relationships between SSA and certain easy-to-measure properties. For instance, particle size distribution (PSD) is widely adopted to calculate SSA by dividing the size distribution of aggregate into several bins and assuming equivalent spherical or polyhedral particles that have the equivalent size of each bin [10,11]. Besides, an equation of the form of $SA = eV^{0.667}$ was proposed by Erdogan [12] where SA is surface area and V is volume while e is a factor related to the dimensions of the particles. However, aggregates are 3D random particles with irregular and diverse shapes. This

* Corresponding authors.

E-mail addresses: jzhw@tongji.edu.cn (Z. Jiang), Geert.DeSchutter@UGent.be (G. De Schutter).

non-equidimensional feature is more remarkable for crushed aggregates like manufactured sand, which is attracting increasing attention as fine aggregate in concrete [13]. Certain correction factors like flakiness & elongation index [14] or surface area factor [15–17] were used to include the influence of particle shape during SSA calculation. However, these methods consider the overall shape influence on SSA but fail to involve the influence of properties like angularity and roughness, both of which increase the tortuosity of particle surface. In addition to the semi-empirical estimations, indirect method was proposed by coating aggregates with a liquid or a powder and comparing the amount of coated substance on aggregate particles with that on the reference having a known surface area [18–20]. However, this method is operator-sensitive and the result is influenced by many factors like aggregate surface features given that different aggregates may have diverse adsorbing performances. Similarly, gas was also used to coat particles to approximate the surface area of solids while Brunauer-Emmett-Teller (BET) method is a most widely used and standardized one [21,22] SSA can be calculated based on the amount of adsorbate on the surface of particles. However, BET method shows higher value since the gas adsorption occurs not only on the external surface but also on the surface of open internal pores. BET result is thus highly influenced by the porosity of aggregates, which may arise from factors like weathering and lithology [23].

Image processing technology is another tool that can be used to approximate the properties of particles based on their two-dimensional (2D) or three-dimensional (3D) images. For instance, scanning electron microscope (SEM) images were used to determine the SSA [17], particle shape and size [24], as well as mineral compositions [25] of cementitious materials based on image analysis. However, these 2D methods cannot be directly used for measuring the SSA of irregular aggregates. In terms of 3D image methods, computed tomography (CT) is a well-developed technology with considerable value in many fields [26–28]. The most remarkable advantage of CT is its ability to quickly image the interior of solid in three dimensions without any destruction [29]. A 3D view of the sample can be obtained by stacking 2D slices. Then the SSA or other geometric features can be measured based on the reconstructed 3D sample. CT can be regarded as the current ultimate testing method for SSA determination of aggregates. In spite of the advantages it offers, CT equipment is relatively costly, its usage for routine analyses is not practical yet. Therefore, CT plays a better role as a benchmark for estimating new testing methods in term of SSA.

It can be summarized that improvement on SSA determination is achieved due to imaging techniques by eliminating human errors. However, 3D image method like CT for the moment seemingly has limited use for daily analyses owing to its capital intensiveness and complicated operation requirement. As a result, it is of great interest to develop a cheaper and easy-to-perform quantification method of SSA with high accuracy, which can be widely used for general analyses.

If particles are randomly distributed, 2D sections could be used to estimate the 3D properties based on the principles of stereology [30]. SSA of aggregates is possibly determined based on 2D images if the number of images is high enough given that CT result is obtained from numerous 2D slices as well. In this paper, a 2D image-based methodology is proposed to measure the SSA by random sectioning of aggregate. The validation of the SSA determination approach is then accomplished by comparing SSA result with that from spherical assumption, BET and CT methods. Besides, the reasons behind the diverse results were discussed. Finally, factors that may influence SSA result of random sectioning method are analyzed. It needs to be mentioned that SSA in this paper refers to the surface area per unit volume of a particle for the

consideration that aggregates with various lithology have different apparent densities.

2. Conventional methods

2.1. Spherical assumption

PSD can be used to approximate SSA by dividing the size distribution of aggregate into several bins and assuming equivalent spherical or polyhedral particles that have the equivalent size of each bin. The SSA based on spherical assumption can be determined as follows.

$$SSA = \frac{F}{\rho} \sum \frac{6f_d}{D} \quad (1)$$

where ρ is the average mass density of particle, f_d is the volume fraction of particles with diameter of D , F is an empirical correction factor 1.13 to consider the particle surface shape [16,17]. In practice, PSD is determined by sieving. D is determined as the geometric mean of maximum and minimum diameters of each bin.

2.2. BET analysis

2.2.1. BET model

The principle of BET test is to quantify the amount of an adsorbate (nitrogen in this study) required to form a closely packed monomolecular layer on the whole surface of solid. This amount can be determined in the low partial pressure region of the adsorption isotherm. In previous investigations, the specific surface area was expressed as the amount of area per mass of particles, shown as follows [31,32].

$$SSA = \frac{V_m N A_m}{22400M} \quad (2)$$

where A_m is the projection area of one vapor molecule which is determined based on the hexagonal close packing model, N is Avogadro constant, and M is the mass of particles.

For comparison with other methods, the specific surface area of BET method is then presented as the amount of area per volume of particles, shown below.

$$SSA = \frac{V_m N A_m \rho}{22400M} \quad (3)$$

where ρ is the apparent density of measured particles.

2.2.2. BET test

BET test was carried out using a BET multi-point nitrogen physisorption equipment (BEISHIDE 3H-2000PS2) [33,34]. Samples were degassed at 105 °C under vacuum for 6 h before adsorption test. The nitrogen adsorption capacity was determined from a six-points adsorption isotherm at 77.3 K in the relative pressure ranging from 0.05 to 0.30. Each sample was measured for three times.

2.3. CT analysis

2.3.1. Principle of CT test

During CT testing, X-rays irradiate a 3D sample from various angles and a detector evaluates the resulting intensity of a known unidirectional (x-axis) X-ray beam intensity due to the absorption by the sample, and for different directions of irradiations [35,36].

According to attenuation measurements over many views (ray paths), a 2D cross-sectional image can be mathematically reconstructed. Then a computer-based reconstruction technique can be used to produce gray images. Each image represents one slice of the sample and the contrast in gray levels is attributed to the

difference of constituents in the sample regarding X-ray absorption capacity. A 3D view of the sample can be obtained if these images are successively stacked together. The SSA can be finally calculated based on the reconstructed 3D structure.

2.3.2. CT test

Tomographic data were obtained using Hector CT scanner at the Center for X-ray Tomography, Ghent University (Belgium) [37]. The raw data (sonograms) were reconstructed into 2D slice images using the in-house developed software package Octopus [38]. The reconstructed voxel dimension is $7^3 \mu\text{m}^3$ based on a source-to-object distance of 41.4 mm and a source-to-detector distance of 1166.0 mm. The reconstructed images comprise 2000×2000 pixels and there are 1500 reconstructed images for one sample.

3D reconstruction was accomplished by using the software Blob3D. The process of 3D reconstruction is illustrated in Fig. 1. Segment procedures like thresholding, median smoothing, Gaussian filtering and islands/holes removing were adopted to define pixels that belong to the object of interest, indicated by the transformation of gray images into binarized images. After the formation of 3D structure by stacking the successive 2D binarized images, 3D particles contact with adjacent ones. Thus, the procedure of separation was performed, like size thresholding, erosion/dilation and plane definition, to separate the reconstructed and connected particles. It is to be noted that erosion/dilation operations may slightly influence the morphology of a particle, thus erosion/dilation operation was used as less as possible. Finally, SSA can be calculated based on the isosurface surrounding the object voxels.

2.3.3. CT result analysis

SSA calculated from various numbers of reconstructed 3D particles is shown in Fig. 2. It is observed that SSA significantly fluctuates for the first 10 particles. Then a sluggish variation of SSA can be seen when more particles are involved. The coefficient of variation of SSA after 60 particles is 1.4% while the maximum relative error of SSA from more than 60 particles to that from 60 particles (superposed in Fig. 2) is 2.0%, where such small values indicate that a relatively constant SSA is available when particle number reaches

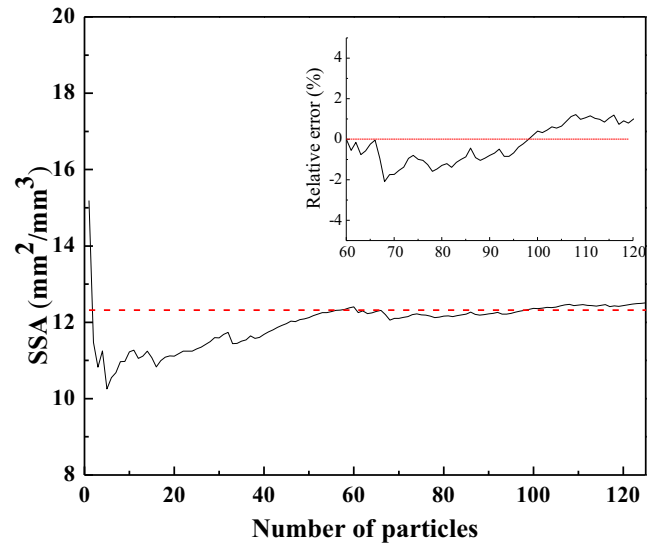


Fig. 2. SSA results measured from CT method based on various number of reconstructed 3D particles.

60. Thus 60 reconstructed particles can be considered sufficient for SSA determination based on CT test, compared to 30 particles in Ref [2].

3. Random sectioning method

3.1. Theoretical background

Random sectioning method was proposed by Smith and Guttman to measure the internal boundaries in 3D structures [39]. This method is employed to calculate the SSA of particles in this study. The derivation of equations for calculating SSA are shown as follows based on references [30,39].

Fig. 3 describes an irregular solid body with closed surface, which is intersected by a stack of parallel planes with a distance

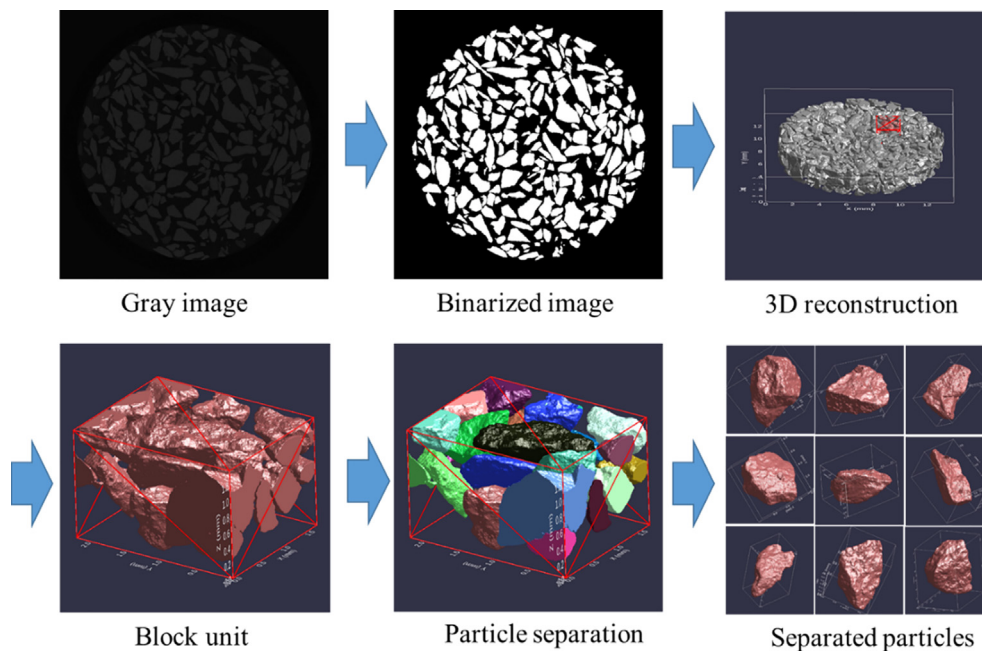


Fig. 1. 3D reconstruction process of CT analysis.

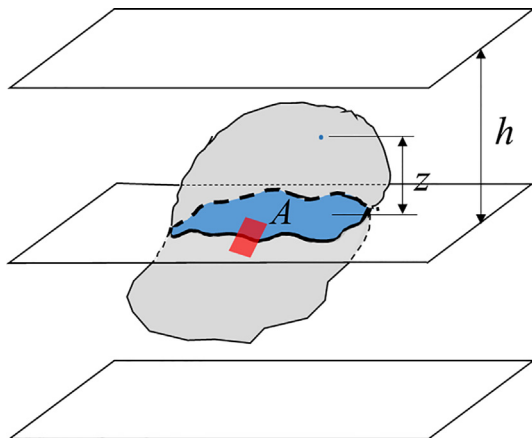


Fig. 3. A solid body intersected by a set of parallel planes.

h . The position of the surface of the object can be defined by the distance z of a fixed point on the aggregate surface to the intersection plane. The orientation of this surface can be described by angle ω for simplicity. The area (A) of the intersection is thus a function of ω and z . The average area (\bar{A}) for all possible positions and orientations of the object, can be determined based on Eq. (4).

$$\bar{A} = \frac{\int d\omega \int dz A(\omega, z)}{\int d\omega \int dz} \quad (4)$$

If the orientation is fixed, $A(\omega, z)dz$ is the volume element of the object.

$$\int_0^d A(\omega, z) dz = V \quad (5)$$

where V is the volume of the object.

Therefore, Eq. (4) can be simplified as Eq. (6), which indicates that the average area of intersection for all possible positions and orientations of the object is the volume of the body divided by the distance of the parallel planes.

$$\bar{A} = \frac{V}{h} \quad (6)$$

Now, we consider a surface element of the object (red area in Fig. 3), which intersects one of the parallel planes. This surface element can be taken as a plane shown in Fig. 4. The length of the intersection is l and its average for all positions and orientations can be expressed as Eq. (7) [39].

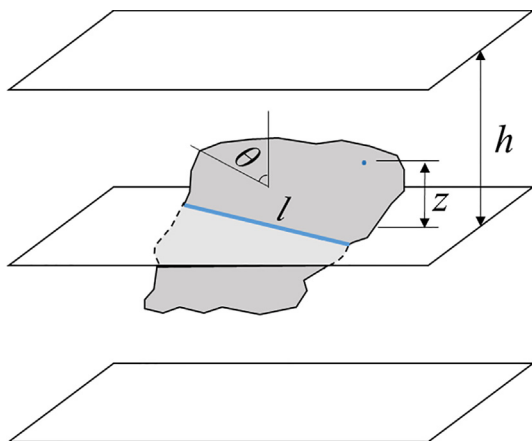


Fig. 4. A unit surface intersected by a set of parallel planes.

$$\bar{l} = \frac{\int d\omega \int dz l(\omega, z)}{\int d\omega \int dz} \quad (7)$$

If the orientation is fixed, ldz is surface element of the figure projection on a certain plane that is normal to the stack of planes and includes the intersection.

$$ldz = dS \sin \theta \quad (8)$$

where θ is the angle between the normal direction of the figure and the normal direction of the parallel planes. Thus, the integration over z presents the total area of the surface projected on the vertical plane. The orientation angle ω can be expressed as follows.

$$d\omega = \sin \theta d\theta \quad (9)$$

The range $(0, \pi/2)$ of θ covers all possible orientations. Thus, Eq. (7) can be specified as Eq. (10).

$$\bar{l} = \frac{S \int_0^{\pi/2} \sin^2 \theta d\theta}{\int_0^{\pi/2} \sin \theta d\theta \int_0^h dz} = \frac{\pi S}{4h} \quad (10)$$

This result is not confined to plane figures given that any surface is constituted by a large number of plane elements. Besides, these elements take random positions and orientations when the figure as a whole dose so. It needs to be mentioned that the contributions to the surface and to the length of intersection are additive. As a result, Fig. 4 holds for any surface. Therefore, the average length (\bar{l}) indicates the average perimeter of all possible sections of the object.

By combining Eqs. (6) and (10), the following equation can be obtained.

$$\frac{\bar{l}}{\bar{A}} = \frac{\pi S}{4V} \quad (11)$$

This result does not depend on h , which indicates that the set of parallel planes are not needed in essence. It is practicable to average the line length and area of the intersections of any solid by a randomly-oriented and -placed plane.

Eq. (11) can be presented as the following one, from which the SSA of a particle can be determined based on the ratio between average perimeter and average area of sections at random positions and orientations. This equation is supposed to be valid for particle mixtures if the number of intersections is large enough.

$$\frac{S}{V} = \frac{4}{\pi} \frac{\bar{l}}{\bar{A}} \quad (12)$$

3.2. Random sectioning test

3.2.1. Sample preparation

Manufactured sand particles between 0.50 mm and 1.00 mm sieve sizes were used in this study (Fig. 5(a)) in view of its significantly irregular geometrical features among aggregates. Sand particles were washed and dried first. Then they were impregnated into epoxy resin (EpoFix Resin™) in a silicon mold with an inner diameter of 20 mm. In order to increase the contrast between objects and background, epoxy resin was blended with 0.5% (mass ratio) fluorescent dye (EpoDye™) and homogenized beforehand. The sample was cured at 40 °C for 24 h to harden. The hardened sample was then ground and polished by a polishing machine (LaboPol-5, Struers) at a rotational speed of 200 rpm using SiC papers #180, #320, #1200 and #2000 successively, during which one-quarter of a turn was made every half a minute for a total of 2 min for each SiC paper. Water was used as the cooling medium. Finally, a smooth surface with abundant exposed particles can be obtained after these procedures, seen in Fig. 5(b). Afterwards, the



Fig. 5. Sand particles (a) and sample for image acquisition (b) under optimal microscope (c).

optical microscope (Leica S8 APO, Fig. 5(c)) with a fluorescent light was used to capture the section image of particles.

3.2.2. Image processing

The objective of image processing is to measure the perimeter and surface of particles on the cross section. The captured image (shown in Fig. 6(a)) was transformed into gray image (Fig. 6(b)) for the convenience of thresholding, which is to identify the objects from the background. There exist several thresholding algorithms [40,41], mainly based on the gray tone level histogram of the image. Among these methods, the minimum error algorithm views the gray level histogram as a probability density function (PDF) of the gray levels of both the object and background ($j = 1, 2$). Besides, each of them is considered to follow a normal distribution with a mean value of $m(j)$, a standard deviation of $\sigma(j)$ and a PDF of $P(j)$.

The PDF of gray level of gray image (Fig. 6(b)) is shown in Fig. 7, where two normally distributed segments are observed with a fitted R^2 of 0.960, which indicates the feature of the minimum error algorithm. Thus, the minimum error algorithm is used in this study. However, the parameters of $m(j)$, $\sigma(j)$ and $P(j)$ are usually unknown. Instead, a criterion function $J(j)$ is employed, expressed as Eq. (13) [42].

$$J(t) = 1 + 2[P_1(t)\text{Ln}\sigma_1(t) + P_2(t)\text{Ln}\sigma_2(t)] - 2[P_1(t)\text{Ln}P_1(t) + P_2(t)\text{Ln}P_2(t)] \quad (13)$$

where $P_1(t)$ is the cumulative probability of gray values less than or equal to t while $P_2(t)$ is the cumulative probability of gray values higher than t , which can be determined according to Eqs. (14) and (15) respectively. $\sigma_1(t)$ is the standard deviation of gray values less than or equal to t while $\sigma_2(t)$ is the standard deviation of gray values higher than t , calculated as Eqs. (16) and (17) respectively.

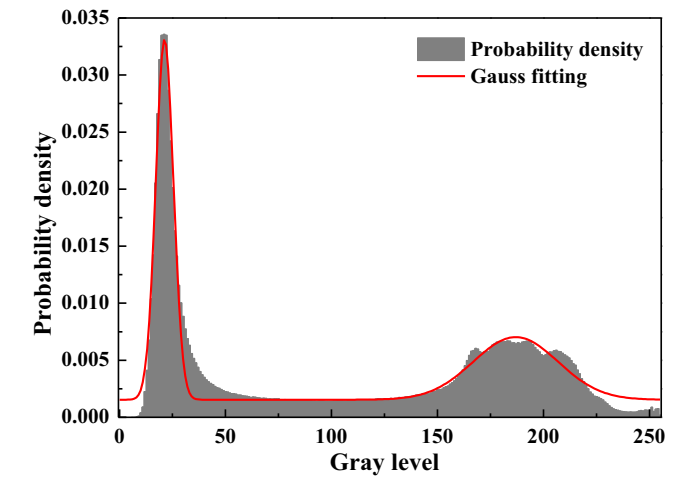


Fig. 7. Probability density of gray level histogram of Fig. 6(b).

$$P_1(t) = \sum_{i=0}^t p(i) \quad (14)$$

$$P_2(t) = \sum_{i=t+1}^{L-1} p(i) = 1 - P_1(t) \quad (15)$$

$$\sigma_1(t) = \frac{1}{P_1(t)} \sum_{i=0}^t [i - m_1(t)]^2 \cdot p(i) \quad (16)$$

$$\sigma_2(t) = \frac{1}{P_2(t)} \sum_{i=t+1}^{L-1} [i - m_2(t)]^2 \cdot p(i) \quad (17)$$

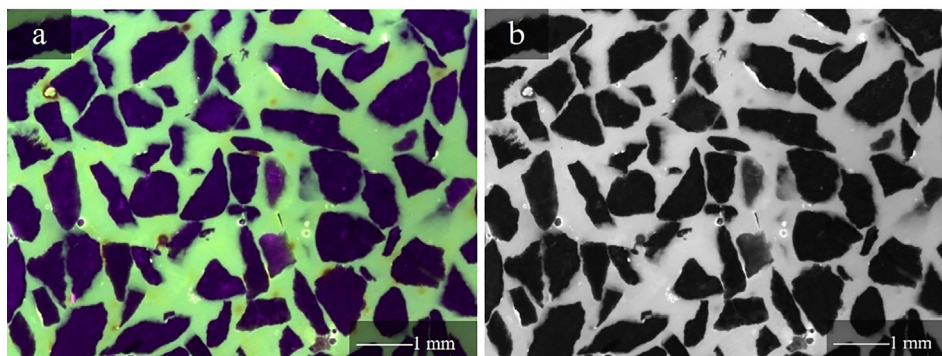


Fig. 6. (a) original and (b) gray images.

where $m_1(t)$ is the mean of gray values less than or equal to t while $m_2(t)$ is the mean of gray values higher than t . $m_1(t)$ and $m_2(t)$ are determined as follows.

$$m_1(t) = \frac{1}{P_1(t)} \sum_{i=0}^t i \cdot p(i) \quad (18)$$

$$m_2(t) = \frac{1}{P_2(t)} \sum_{i=t+1}^{L-1} i \cdot p(i) \quad (19)$$

The optimal threshold t^* is then determined by minimizing $J(t)$, as described in Eq. (20).

$$J(t^*) = \min_{t \in GL} J(t) \quad (20)$$

The gray image can be transformed into a binary image with the determined threshold value, which identifies the objects from the background. Then numbers of pixels representing particles and their boundaries are available by the software MATLAB. Therefore, the SSA of the particles can be calculated from (21).

$$\frac{S}{V} = \frac{4}{\pi} \frac{N_p}{N_A L_0} \quad (21)$$

where N_A and N_p are the numbers of pixels corresponding to objects and their boundaries, L_0 is the edge length of each pixel.

4. Comparison and discussion

The SSA results from spherical assumption, BET, CT and random sectioning methods are exhibited in Table 1. It is clear that SSA from BET is one order or two orders of magnitude higher than SSA from the other methods while the SSA calculated based on the spherical assumption shows the lowest value. However, it is to be noted that CT and random sectioning methods provide very similar results.

Spherical assumption fails to consider the influence of complex geometrical features of particles on SSA. For particles with various shapes, centrosymmetric particle with smooth surface (perfect sphere) has the lowest specific surface area while SSA increases if the particle is deviating from central symmetry or if the surface becomes rougher [11,12]. This means that the spherical assumption underestimates the SSA of real particles and the employed correction factor is too small to capture the influence of particle shape. Even though Platonic shapes like tetrahedron, cube, icosahedron, dodecahedron and octahedron were ever employed to mitigate the particle shape influence on SSA evaluation, regular shape assumption cannot be used to accurately calculate the SSA of irregular aggregate given that the influence of geometric features on the SSA is not predictable due to the irregular feature. In the case of BET method, the surface of open inner pores of particles is also counted in for SSA calculation in addition to their external surface area. Thus, BET is considered to overestimate the SSA of particles and this effect is especially significant for particles with porous structures.

CT and random sectioning methods are direct visual analysis methods while CT is based on 3D reconstructed particle shape and random sectioning method is based on the statistical data from numerous 2D sections. It needs to be mentioned that SSA is not only influenced by the overall shape of particles, but also affected by surface features like roughness, which is typically considered to

be the high-frequency, short-wavelength component of a measured surface. Theoretically, CT and random sectioning methods are supposed to theoretically consider any geometrical shapes, depending on their voxel or pixel size.

There is no doubt that CT is the most accurate method to verify new methods if the resolution is proper given that there are a lot of factors like assumptions and degassing conditions, influencing the result of BET methods [17,43]. From the viewpoint of resolution, we can take the surface of a particle as the combination of huge numbers of small pixels. The resolution of BET method is approximately the diameter of one N_2 molecule (around 0.4 nm) while the resolutions of CT and random sectioning methods depend on the resolution of equipment (CT scanner and optical microscope respectively) or/and user's selection, 7 μm and 4 μm respectively in this paper. When the resolution is too low, the roughness is unable to be captured and SSA is underestimated. However, an overestimated SSA will be provided if the pixel is too small due to "roughness" induced by pixilation. This explains why BET method shows much higher SSA than other methods. To sum up, it is necessary to determine the scale at which the features of the surface are intended to be captured before selecting the optimal testing method.

It is considered that 3D image methods are supposed to measure the SSA at a higher accuracy than 2D image methods due to the fact that 3D methods are able to capture the surface features on the third dimension. However, if the number of 2D sections is high enough, this influence can be alleviated. Besides, a lot of testing steps and image processing procedures were performed on samples to obtain data for SSA calculation and a lot of parameters were selected during image processing, especially for CT method. Each procedure and parameter affects the SSA result. From this viewpoint, more deviations are likely to be employed during image processing of CT method. As a whole, random sectioning method provides similar result with CT test while their resolutions are comparable. Since the 'real' surface area of the sample is not available, the accuracy of these two methods cannot be evaluated. However, in general, CT is well considered to be able to accurately measure the SSA. Thus, random sectioning method can be taken as a reliable method compared to CT.

5. Influence factors on SSA results of random sectioning method

This section is to analyze the factors that may influence SSA results, including the number of particles used for calculation, threshold value and the resolution of pixel.

5.1. Number of particles

Number of particles should be large enough to present intersections at random positions and from random orientations, indicated by a steady SSA result. Fig. 8 shows the SSA results calculated from various numbers of particles. It is seen that SSA presents rather fluctuating value within the first few tens of particles and then shows increasingly steady results as the number of particles increases. To be specific, SSA in the range of 12 mm^2/mm^3 to 13 mm^2/mm^3 can be noticed if more than 400 particles are used. In addition, the coefficient of variation of SSA from 800 to 1500 particles is 0.4% while the maximum relative error of SSA from more than 800 particles to that from 800 particles (i.e. SSA/

Table 1
SSA results from different methods (mm^2/mm^3).

Methods	Spherical assumption	BET	CT	Random sectioning
SSA	9.6	329.7	12.6	12.2

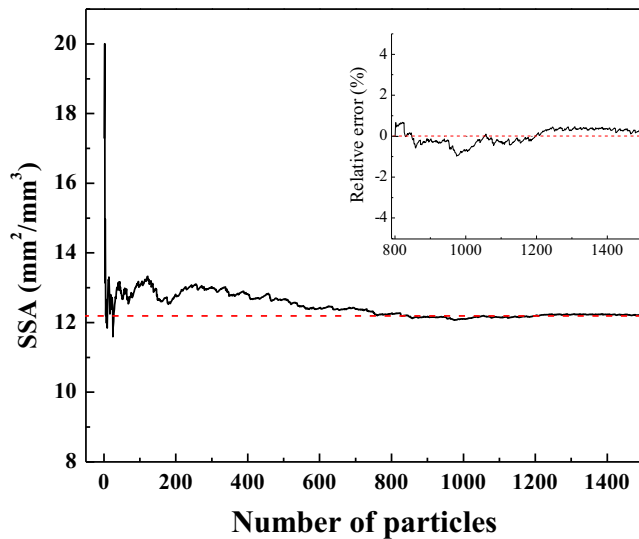


Fig. 8. SSA results versus the number of particles used for calculation.

SSA_{800-1} , superposed in Fig. 8) is 1.0%, where such a small error means a rather steady SSA without obvious variation is reached from 800 particles. As a result, we believe that 800 particles are sufficient to approach the steady SSA based on random sectioning method for the tested manufactured sand particles.

It needs to be mentioned that the number of particles for a steady SSA result depends on the dispersity of particle shape and particle size. A larger number of particles are required when particles have higher dispersity in shape and a wider particle size distribution.

5.2. Threshold value

Thresholding is a vital procedure for image processing. Various threshold values ranging from 20 to 200 were used for image processing and SSA were calculated as shown in Fig. 9. In general, SSA decreases with the increase of gray level. SSA shows a dramatic decrease before a critical value, followed by a sluggish decrease after this critical value. This critical value is considered to be the threshold value, which is 40 for the gray image (Fig. 6) according to the minimum error algorithm (see above). The binary images after thresholding at 30, 40 and 100 are shown in Fig. 10. It is

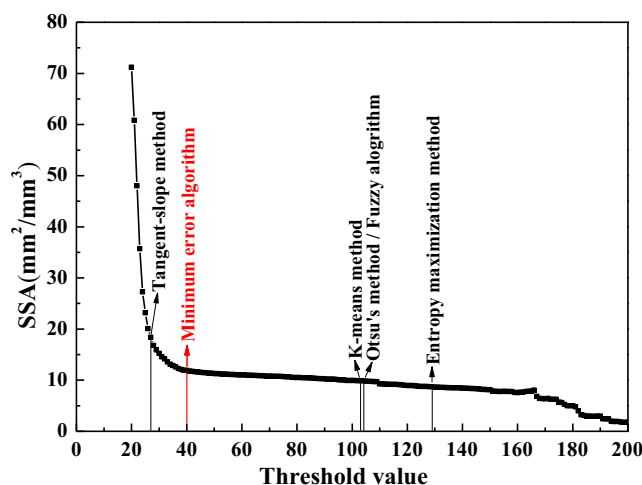


Fig. 9. SSA results and threshold values from several commonly used thresholding methods.

observed that when threshold is smaller than the critical value (Fig. 10a), particles were partially eroded, making boundaries more tortuous. Erosion decreases the area of objects and increases their perimeter at the same time. This influence is supposed to be more significant when thresholding value further decreases. As a result, SSA sharply increases with the decreasing threshold value before the critical point. However, the increase of threshold value after the critical point dilates the particles (Fig. 10c), which overestimates the area of objects on one hand. On the other hand, objects will merge with the adjacent ones, resulting in loss of perimeter. Thus, the SSA is decreasing with the increase of threshold value. This influence is gentler, indicated by the sluggish decreasing trend. In addition to the minimum error algorithm, other commonly used thresholding methods including tangent-slope method [44], K-means method [40], Otsu's method [45], fuzzy algorithm [46] and entropy maximization method [47] were also tried and the determined threshold values are also superposed in Fig. 9. It is observed that different thresholding methods provide diverse threshold values, ranging from 27 to 129. For the bimodal histogram of gray level in this paper, various algorithms are expected to provide similar threshold values around the valley between the peaks of foreground histogram and background histogram. However, this valley is quite wide and flat according to Fig. 7. Minor differences between the algorithms can make the resultant threshold values vary a lot. As a result, compared with SSA based on the minimum error algorithm, the tangent-slope method shows 54.2% higher while K-means method, Otsu's method, fuzzy algorithm and entropy maximization method respectively present 17.0%, 17.1%, 17.1% and 27.0% lower SSA results than that from the minimum error algorithm.

5.3. Resolution of pixel

A proper resolution is desired for image analysis. Fig. 11 shows the SSA variation with the resolution of pixel. It needs to be mentioned that a smaller pixel size requires more particles for an unbiased estimation. SSA results in Fig. 11 are obtained based on sufficient particles for each resolution of pixel. It is clear that SSA exhibits an increasing trend with the increase of resolution (decrease of pixel size). Specifically, SSA shows 24.0%, 35.8%, 54.0%, 55.5% and 56.6% higher values when the resolution increases from 128 $\mu\text{m}/\text{pixel}$ to 64 $\mu\text{m}/\text{pixel}$, 32 $\mu\text{m}/\text{pixel}$, 16 $\mu\text{m}/\text{pixel}$, 8 $\mu\text{m}/\text{pixel}$, and 4 $\mu\text{m}/\text{pixel}$, respectively. This trend is attributed to the fact that a higher resolution captures more details on the geometrical shape like surface texture.

It can be seen in Fig. 12 that boundaries information is increasingly clear when the resolution is gradually improved. Therefore, the resolution should be as high as possible for SSA determination when the geometrical features at smaller scale are expected to be considered. However, it is also noted that SSA shows a sluggish increase when the resolution is higher than 16 $\mu\text{m}/\text{pixel}$. Specifically, SSA increases by 2.8% when the resolution increases from 16 $\mu\text{m}/\text{pixel}$ to 8 $\mu\text{m}/\text{pixel}$. Further improvement of resolution from 8 $\mu\text{m}/\text{pixel}$ to 4 $\mu\text{m}/\text{pixel}$ provides 2.0% higher SSA value. Therefore, a resolution higher than 16 $\mu\text{m}/\text{pixel}$ provides relatively reliable SSA result while 4 $\mu\text{m}/\text{pixel}$ is used in this study if not specified otherwise. In engineering practice, the balance between pixel size and number of particles should be made to make the result reliable with both pixel size and number of particles considered.

6. Conclusion

Random sectioning method was proposed for the determination of SSA of irregular-shaped aggregate. For validation, conventional



Fig. 10. Binary images after thresholding at (a) 30, (b) 40 and (c) 100.

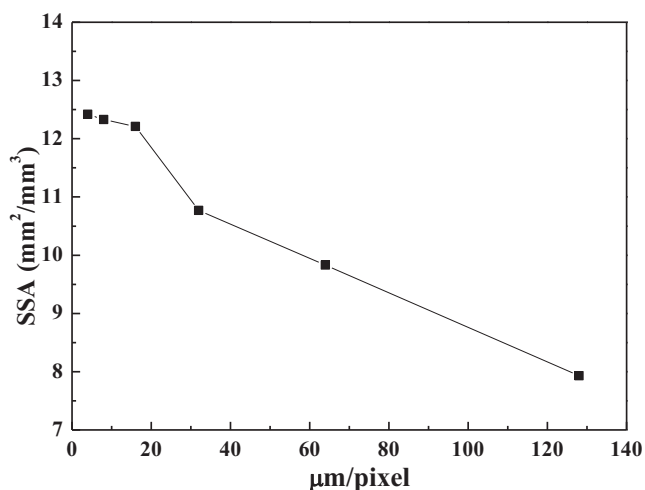


Fig. 11. SSA results under various resolutions.

methods including spherical assumption, BET and CT methods were used for comparison. Factors that possibly influence SSA result were analyzed, like number of particles, threshold value and the resolution of pixel.

Spherical assumption provides the lowest SSA result due to the fact that the influence of irregular geometric features on SSA is not considered. BET method measures the surface that nitrogen molecule can reach and be adsorbed on in the relative pressure range of 0.05 to 0.30, including open pore surface. This method approximates the SSA based on the ‘pixel’ of nitrogen molecule. As a result, BET method provides one order of magnitude higher SSA than the other three methods.

Both CT and random sectioning measure the SSA of particles based on direct visual analysis. Random sectioning method provides very similar result with CT test and can be considered as a reliable method compared to CT result in terms of accuracy.

Besides, the implementation of random sectioning method is simple, independent of expensive equipment and complicated operations.

In practice of SSA determination, it is necessary to determine the scale at which the features of surface are supposed to be captured before selecting the optimal testing method.

CRedit authorship contribution statement

Qiang Ren: Conceptualization, Methodology, Investigation, Formal analysis, Writing - original draft. **Luchuan Ding:** Methodology, Writing - review & editing. **Xiaodi Dai:** Formal analysis, Writing - review & editing. **Zhengwu Jiang:** Conceptualization, Writing - review & editing. **Guang Ye:** Formal analysis, Writing - review & editing. **Geert De Schutter:** Methodology, Writing - review & editing.

Declaration of Competing Interest

The authors declare that they have no known competing financial interests or personal relationships that could have appeared to influence the work reported in this paper.

Acknowledgements

The authors acknowledge the financial supports provided by National Key Research and Development Projects (2018YFC0705404), National Natural Science Foundation of China (51878480, 51878479, 51678442, 51878481 and 51878496) and the Fundamental Research Funds for the Central Universities. Authors gratefully acknowledge the Centre for X-ray Tomography of Ghent University for its support on CT test.

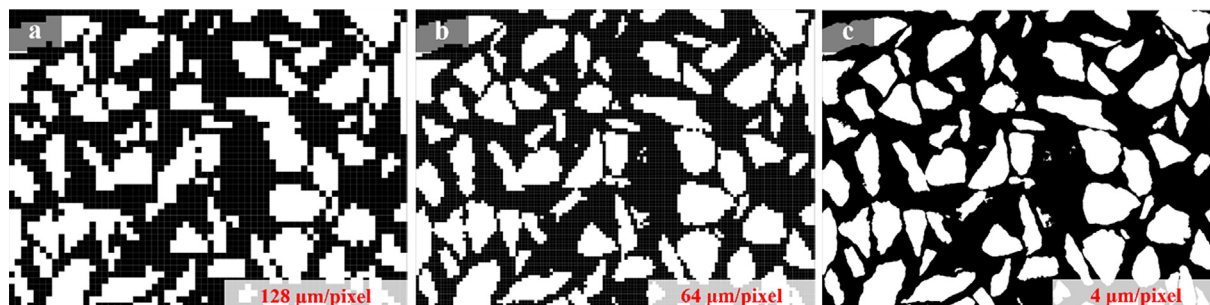


Fig. 12. Binary images with resolutions of (a) 128 µm/pixel, (b) 64 µm/pixel and (c) 4 µm/pixel.

References

- [1] M.R. Mitchell, R.E. Link, D.Q. van Lent, A.A.A. Molenaar, M.F.C. van de Ven, M. van de Ven, Influence treatment in laboratory of stone surface on the surface roughness, *J. Test. Eval.* 37 (5) (2009) 000017.
- [2] L. Wang, J. Frost David, Quantification of the specific aggregate surface area using X-ray tomography, in: E. Tutumluer, Y.M. Najjar, E. Masad (Eds.) 15th Engineering Mechanics Division Conference, ASCE, New York, United States, 2002, pp. 3–17. [http://doi.org/10.1061/40709\(257\)1](http://doi.org/10.1061/40709(257)1).
- [3] A.K.H. Kwan, L.G. Li, Combined effects of water film, paste film and mortar film thicknesses on fresh properties of concrete, *Constr. Build. Mater.* 50 (2014) 598–608, <https://doi.org/10.1016/j.conbuildmat.2013.10.014>.
- [4] H. Li, H. Zhang, L. Li, Q. Ren, X. Yang, Z. Jiang, Z. Zhang, Utilization of low-quality desulfurized ash from semi-dry flue gas desulfurization by mixing with hemihydrate gypsum, *Fuel* 255 (2019) 115783.
- [5] Q. Ren, M. Xie, X. Zhu, Y. Zhang, Z. Jiang, Role of limestone powder in early-age cement paste considering fineness effects, *J. Mater. Civ. Eng.* 32 (10) (2020) 04020289, [https://doi.org/10.1061/\(ASCE\)MT.1943-5533.0003380](https://doi.org/10.1061/(ASCE)MT.1943-5533.0003380).
- [6] C.F. Goble, M.D. Cohen, Influence of aggregate surface area on mechanical properties of mortar, *ACI Mater. J.* 96 (6) (1999) 657–662.
- [7] X. Yang, J. Liu, H. Li, Q. Ren, Performance and ITZ of pervious concrete modified by vinyl acetate and ethylene copolymer dispersible powder, *Constr. Build. Mater.* 235 (2020) 117532.
- [8] K. Wu, H.S. Shi, L.L. Xu, G. Ye, G. De Schutter, Microstructural characterization of ITZ in blended cement concretes and its relation to transport properties, *Cem. Concr. Res.* 79 (2016) 243–256, <https://doi.org/10.1016/j.cemconres.2015.09.018>.
- [9] M. Alexander, S. Mindess, *Aggregates in concrete*, CRC Press, 2010.
- [10] Y. Ghasemi, M. Emborg, A. Cwirzen, Exploring the relation between the flow of mortar and specific surface area of its constituents, *Constr. Build. Mater.* 211 (2019) 492–501, <https://doi.org/10.1016/j.conbuildmat.2019.03.260>.
- [11] Y. Ghasemi, M. Emborg, A. Cwirzen, Estimation of specific surface area of particles based on size distribution curve, *Mag. Concr. Res.* 70 (10) (2018) 533–540, <https://doi.org/10.1680/jmacr.17.00045>.
- [12] S.T. Erdogan, Simple estimation of the surface area of irregular 3D particles, *J. Mater. Civ. Eng.* 28 (8) (2016) 10, [https://doi.org/10.1061/\(asce\)mt.1943-5533.0001575](https://doi.org/10.1061/(asce)mt.1943-5533.0001575).
- [13] Q. Ren, G. De Schutter, Z. Jiang, Q. Chen, Multi-level diffusion model for manufactured sand mortar considering particle shape and limestone powder effects, *Constr. Build. Mater.* 207 (2019) 218–227, <https://doi.org/10.1016/j.conbuildmat.2019.02.139>.
- [14] R.P. Panda, S.S. Das, P.K. Sahoo, An empirical method for estimating surface area of aggregates in hot mix asphalt, *J. Traffic Transp. Eng.-Engl. Ed.* 3 (2) (2016) 127–136, <https://doi.org/10.1016/j.jtte.2015.10.007>.
- [15] J. Anochie-Boateng, J. Komba, E. Tutumluer, 3D laser based measurement of mineral aggregate surface area for south African hot-mix asphalt mixtures, Transportation Research Board 90th Annual Meeting, United States, Washington DC, 2011.
- [16] H.F. Taylor, *Cement chemistry*, Thomas Telford London, 1997.
- [17] T. Wang, T. Ishida, R. Gu, A comparison of the specific surface area of fly ash measured by image analysis with conventional methods, *Constr. Build. Mater.* 190 (2018) 1163–1172, <https://doi.org/10.1016/j.conbuildmat.2018.09.131>.
- [18] P.C. Knodel, V.K. Garga, R. Townsend, D. Hansen, A method for determining the surface area of quarried rocks, *Geotech. Test. J.* 14 (1) (1991) 35.
- [19] L. Xiao, D. Jiang, The study of pervious concrete mix proportion by the method of specific surface area of aggregate, *IOP Conf. Ser. Mater. Sci. Eng.* 231 (2017) 012094.
- [20] D. Sun, H. Shi, K. Wu, S. Miramini, B. Li, L. Zhang, Influence of aggregate surface treatment on corrosion resistance of cement composite under chloride attack, *Constr. Build. Mater.* 248 (2020) 118636.
- [21] I. Odler, The BET-specific surface area of hydrated Portland cement and related materials, *Cem. Concr. Res.* 33 (12) (2003) 2049–2056, [https://doi.org/10.1016/S0008-8846\(03\)00225-4](https://doi.org/10.1016/S0008-8846(03)00225-4).
- [22] ISO, 15901, Determination of the specific surface area of solids by gas adsorption – BET method, International Organization for Standardization (2010).
- [23] R. Cepuritis, B.J. Wigum, E.J. Garboczi, E. Mørtzell, S. Jacobsen, Filler from crushed aggregate for concrete: Pore structure, specific surface, particle shape and size distribution, *Cem. Concr. Compos.* 54 (2014) 2–16, <https://doi.org/10.1016/j.cemconcomp.2014.03.010>.
- [24] E.C. Arvaniti, M.C.G. Juenger, S.A. Bernal, J. Duchesne, L. Courard, S. Leroy, J.L. Provis, A. Klemm, N. De Belie, Determination of particle size, surface area, and shape of supplementary cementitious materials by different techniques, 48 (11) (2015) 3687–3701. <http://doi.org/10.1617/s11527-014-0431-3>.
- [25] P.T. Durdziński, C.F. Dunant, M.B. Haha, K.L. Scrivener, A new quantification method based on SEM-EDS to assess fly ash composition and study the reaction of its individual components in hydrating cement paste, *Cem. Concr. Res.* 73 (2015) 111–122, <https://doi.org/10.1016/j.cemconres.2015.02.008>.
- [26] R.A. Ketcham, W.D. Carlson, Acquisition, optimization and interpretation of X-ray computed tomographic imagery: applications to the geosciences, *Comput. Geosci-UK* 27 (4) (2001) 381–400, [https://doi.org/10.1016/S0098-3004\(00\)00116-3](https://doi.org/10.1016/S0098-3004(00)00116-3).
- [27] M.A. Taylor, E.J. Garboczi, S.T. Erdogan, D.W. Fowler, Some properties of irregular 3-D particles, *Powder Technol.* 162 (1) (2006) 1–15, <https://doi.org/10.1016/j.powtec.2005.10.013>.
- [28] R. Cepuritis, E.J. Garboczi, C.F. Ferraris, S. Jacobsen, B.E. Sørensen, Measurement of particle size distribution and specific surface area for crushed concrete aggregate fines, *Adv. Powder Technol.* 28 (3) (2017) 706–720, <https://doi.org/10.1016/j.apt.2016.11.018>.
- [29] W.D. Carlson, T. Rowe, R.A. Ketcham, M.W. Colbert, F. Mees, R. Swennen, M.V. Geet, P. Jacobs, Applications of high-resolution X-ray computed tomography in petrology, meteoritics and palaeontology, Applications of X-ray Computed Tomography in the Geosciences, Geological Society of London (2003) 7–22, <https://doi.org/10.1144/gsl.Sp.2003.215.01.02>.
- [30] P.R. Mouton, *Unbiased stereology: A concise guide*, The Johns Hopkins University Press, USA, 2011.
- [31] S. Brunauer, P.H. Emmett, E. Teller, Adsorption of gases in multimolecular layers, *J. Am. Chem. Soc.* 60 (2) (1938) 309–319, <https://doi.org/10.1021/ja01269a023>.
- [32] D. Zhang, R. Luo, Modifying the BET model for accurately determining specific surface area and surface energy components of aggregates, *Constr. Build. Mater.* 175 (2018) 653–663, <https://doi.org/10.1016/j.conbuildmat.2018.04.215>.
- [33] Q. Ren, Z. Zeng, Z. Jiang, H. Li, Functionalization of renewable bamboo charcoal to improve indoor environment quality in a sustainable way, *J. Clean. Prod.* 246 (2020) 119028.
- [34] Q. Ren, Z. Zeng, M. Xie, Z. Jiang, Cement-based composite with humidity adsorption and formaldehyde removal functions as an indoor wall material, *Constr. Build. Mater.* 247 (2020) 118610.
- [35] T.J. Chotard, M.P. Boncoeur-Martel, A. Smith, J.P. Dupuy, C. Gault, Application of X-ray computed tomography to characterise the early hydration of calcium aluminate cement, *Cem. Concr. Compos.* 25 (1) (2003) 145–152, [https://doi.org/10.1016/S0958-9465\(01\)00063-4](https://doi.org/10.1016/S0958-9465(01)00063-4).
- [36] E.N. Landis, D.T. Keane, X-ray microtomography, *Mater. Charact.* 61 (12) (2010) 1305–1316, <https://doi.org/10.1016/j.matchar.2010.09.012>.
- [37] B. Masschaele, M. Dierick, D.V. Loo, M.N. Boone, L. Brabant, E. Pauwels, V. Cnudde, L.V. Hoorebeke, HECTOR: A 240kV micro-CT setup optimized for research, *J. Phys. Conf. Ser.* 463 (2013) 012012.
- [38] J. Vlassenbroeck, M. Dierick, B. Masschaele, V. Cnudde, L. Hoorebeke, P. Jacobs, Software tools for quantification of X-ray microtomography, *Nucl. Instrum. Methods Phys. Res. Sect. A-Accel. Spectrom. Dect. Assoc. Equip.* 580 (1) (2007) 442–445, <https://doi.org/10.1016/j.nima.2007.05.073>.
- [39] C.S. Smith, L. Guttman, Measurement of internal boundaries in three-dimensional structures by random sectioning, *J. Met.* 5 (1) (1953) 81–87, <https://doi.org/10.1007/bf03397456>.
- [40] U. Gonzales-Barron, F. Butler, A comparison of seven thresholding techniques with the k-means clustering algorithm for measurement of bread-crumbs features by digital image analysis, *J. Food Eng.* 74 (2) (2006) 268–278, <https://doi.org/10.1016/j.jfoodeng.2005.03.007>.
- [41] M. Coster, J.-L. Chermant, Image analysis and mathematical morphology for civil engineering materials, *Cem. Concr. Compos.* 23 (2) (2001) 133–151, [https://doi.org/10.1016/S0958-9465\(00\)00058-5](https://doi.org/10.1016/S0958-9465(00)00058-5).
- [42] J. Kittler, J. Illingworth, On threshold selection using clustering criteria, *IEEE T. Syst. Man Cy-S SMC-15* (5) (1985) 652–655.
- [43] S. Mantellato, M. Palacios, R.J. Flatt, Reliable specific surface area measurements on anhydrous cements, *Cem. Concr. Res.* 67 (2015) 286–291, <https://doi.org/10.1016/j.cemconres.2014.10.009>.
- [44] H.S. Wong, M.K. Head, N.R. Buenfeld, Pore segmentation of cement-based materials from backscattered electron images, *Cem. Concr. Res.* 36 (6) (2006) 1083–1090, <https://doi.org/10.1016/j.cemconres.2005.10.006>.
- [45] N. Otsu, A threshold selection method from gray-level histograms, *IEEE T. Syst. Man Cy-S* 9 (1) (1979) 62–66, <https://doi.org/10.1109/TSMC.1979.4310076>.
- [46] L.-K. Huang, M.-J.-J. Wang, Image thresholding by minimizing the measures of fuzziness, *Pattern Recogn.* 28 (1) (1995) 41–51, [https://doi.org/10.1016/0031-3203\(94\)E0043-K](https://doi.org/10.1016/0031-3203(94)E0043-K).
- [47] J.N. Kapur, P.K. Sahoo, A.K.C. Wong, A new method for gray-level picture thresholding using the entropy of the histogram, *Comput. Vision Graph. Image Process.* 29 (3) (1985) 273–285, [https://doi.org/10.1016/0734-189X\(85\)90125-2](https://doi.org/10.1016/0734-189X(85)90125-2).